Langmuir probe electronics upgrade on the Tokamak à Configuration Variable

H. De Oliveira,[1, a)] P. Marmillod,[1] C. Theiler,[1] R. Chavan,[1] O. Février,[1] B. Labit,[1] P. Lavanchy,[1] B. Marlétaz,[1] R. A. Pitts,[2] and the TCV team[3]

[1)] *Ecole Polytechnique Fédérale de Lausanne (EPFL), Swiss Plasma Center (SPC), CH-1015 Lausanne, Switzerland*

[2)] *ITER Organization, Route de Vinon sur Verdon, CS90 046, 13067 St Paul Lez Durance, Cedex, France*

[3)] *See author list of S. Coda et al 2017 Nucl. Fusion 57 102011*

(Dated: 19 July 2019)

A detailed description of the Langmuir probe electronics upgrade for TCV (*Tokamak à Configuration Variable*) is presented. The number of amplifiers and corresponding electronics has been increased from 48 to 120 in order to simultaneously connect all of the 114 Langmuir probes currently mounted in the TCV divertor and main-wall tiles. Another 108 amplifiers are ready to be installed in order to connect 80 new probes, built in the frame of the TCV divertor upgrade. Technical details of the amplifier circuitry are discussed as well as improvements over the first generation of amplifiers developed at SPC (formerly CRPP) in 1993/1994 and over the second generation developed in 2012/2013. While the new amplifiers have been operated successfully for over a year, it was found that their silicon power transistors can be damaged during some off-normal plasma events. Possible solutions are discussed.

I. INTRODUCTION

An extensive array of diagnostics is installed on TCV [1] [2], (*Tokamak à Configuration Variable*) in order to give the most complete and accurate description possible of the plasma. Among the edge diagnostics, Langmuir probes (LP) are one of the most common tools to describe local properties in the boundary region of the plasma [3] [4] [5]. They typically provide measurements of ion saturation current I_{sat}, electron density n_e, electron temperature T_e, floating potential V_{fl} and plasma potential V_{pl}. In the single probe arrangement (local measurement of the plasma properties), I_{sat}, V_{fl} and ion Mach number M can be readily measured with high time response, e.g. 200 kHz or higher. On the contrary, T_e, V_{pl} and n_e are usually obtained by relatively slow sweeping of the probe voltage, resulting in a time response of typically 1 kHz or lower. A detailed description of the analysis and interpretation of LPs in different experimental conditions on TCV has recently been presented elsewhere for wall-embedded probes [6] and for the pins of a fast-reciprocating probe [7].

The main purpose of this paper is to present a newly developed amplifier circuitry to operate single LPs on TCV with an arbitrary bias-waveform or in floating potential mode. Compared to the first generation of custom-built amplifiers on TCV, the new circuitry features an improved amplification final stage with simpler and cheaper components, an improved current measurement and a custom current limitation system based on suspended OP-amps. 180 of these third generation amplifiers have been built and tested, extending the total number of amplifier from 48 to 228 units. This upgrade allows the simultaneous operation of all the 114 wall-embedded single LPs currently installed on TCV [6], as shown in FIG 1, and thus substantially improves the operational flexibility. The upgrade also provides the spare amplifiers necessary to extend the wall LP array in view of the upcoming TCV divertor upgrade [8] [9].

This paper is organized as follows. A short description of the TCV wall-embedded LP design and the transmission lines connecting them to the amplifiers is presented in Sec. II. The design of the new amplifier circuitry is presented in detail in Sec. III, discussing in particular the amplification, the current limitation, and the voltage and current measurement circuit. Protection strategies against amplifier damage are discussed in Sec.IV, followed by a description of the TCV probe coverage planned for the TCV upgrade in baffled and non-baffled configurations in Sec.V. Finally, a summary of the paper is presented in Sec. VI.

II. DESIGN OF THE LANGMUIR PROBES AND CHARACTERISTICS OF THE TRANSMISSION LINE

Langmuir probes have been present in TCV since 1992 [10]. Those are different from the first versions and only the most recent design is presented in this paper. Details of the spatial location of installed probes have been given in 2003 [11] and the different probe tip geometries used in TCV have been described recently [6].

The probe assembly is housed in the TCV polycrystalline graphite tiles which armor the main wall and the divertor, as shown in FIG. 2. Electrical contact is provided by nickel based alloy springs ($R \approx 1\ \Omega$) positioned between the inner conductor of the mineral insulated coaxial cable 1 $Zs\ Ac$ 10 from the company Thermocoax® and the probe tips are manufactured in polycrystalline graphite SGL® Sigrafine $R6650$. The springs used to be made out of copper beryllium alloy with high electrical conductivity ($R \approx 0.1\ \Omega$) and

[a)] hugo.deoliveira@epfl.ch

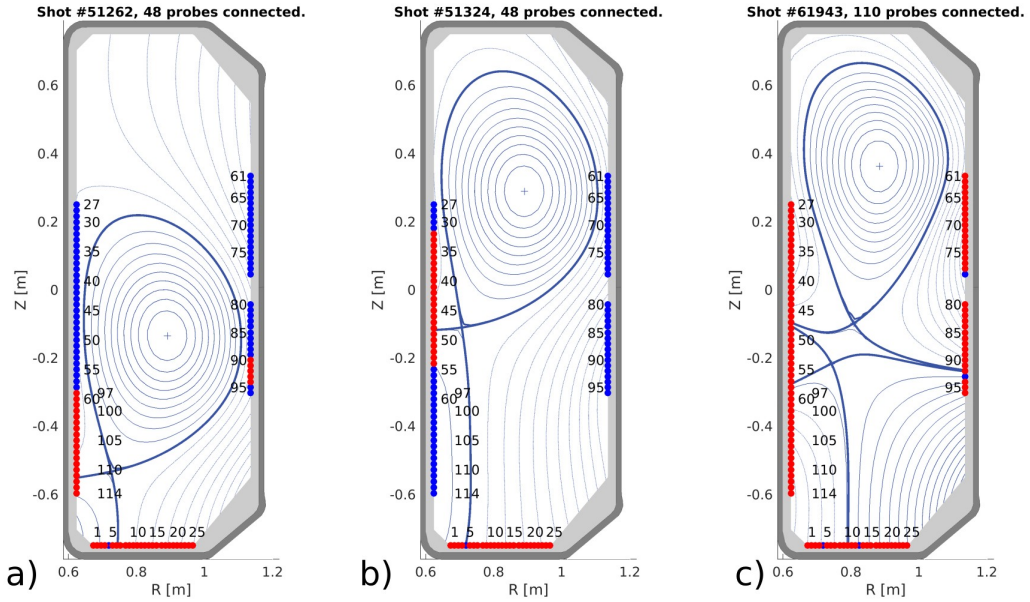

FIG. 1. Poloidal cross-section of TCV with the location of the 114 Langmuir probe tips (red and blue dots). Before the electronics upgrade, the amplifiers needed to be re-wired manually to accommodate the different plasma shapes and positions as shown in **a)** for the shot #51262 and in **b)** for the shot #51324. After the electronics upgrade, e.g. in **c)**, shot #61943, full coverage is attained.

were later discarded: some springs lost their shape because of the annealing process happening at high temperatures. The measured electrical resistance of the assembly ($R \approx 0.5\ \Omega$) is often lower than the resistance of the nickel based alloy springs because the current can find a direct path from the stainless steel housing ④ in FIG. 2 to the copper beryllium finger electrical contact ③ in FIG. 2. If the current goes through the nickel based alloy spring, the electrical resistance of the assembly is $\approx 1.4\ \Omega$. Adding copper springs in parallel with the nickel based alloy springs and electro-deposition of copper on top of the nickel based alloy springs are possible solutions considered for future installations in order to reduce the electrical resistance of this component. The mechanical link between the probe tips and the assembly is assured by the same spring.

Probe tip maintenance requires the tiles to be unfastened and taken out of the machine, as illustrated in FIG. 3 **a)**. The ease of replacement, thanks to the spring assembly, is important to minimize the down-time during manned entries in TCV. Langmuir probe tips need to be replaced when the erosion is large enough to reduce their projected area along the magnetic field. Furthermore, it was observed during the 2019 opening that a resistive layer has been deposited on most probe tips surfaces. The contact resistance measured with round-shaped electrodes is high ($R_{contact} \approx 100\ \Omega$) when the voltage applied is within $\pm 1.7\ V$ and then suddenly drops ($R_{contact} \approx 0.6\ \Omega$) once the applied voltage is larger than $\pm 1.7\ V$, showing variable resistance behavior. It is difficult to evaluate the effective resistance as seen by the plasma, probably an order of magnitude lower than the measured contact resistance because of the larger contact area wetted by the plasma. Such resistive layers can affect the evaluation of the electron temperature [6], particularly in the case of low electron temperature, where the most important part of the IV curve is found in a limited voltage range. It is believed that both carbon redeposition and boronisation play a role in their formation. The resistive layer is supposedly very thin since a gentle sanding with a scouring pad enabled to recover both proper electrical conductance and dull appearance. High heat flux from the plasma can have the same effect as sanding: eroded probes frequently found in the near scrape-off-layer have the characteristic dull appearance from pure graphite and show negligible contact resistance.

Specific care is required when making the Thermocoax® cable termination in order to ensure ultra-high vacuum (UHV) compatibility and proper electrical connection. The magnesium oxide ceramic powder electrical insulation in the Thermocoax® cable acts as a moisture reservoir and therefore the cables must be oven dried before the connectors are brazed to seal the cable terminations. Moisture is problematic because the magnesium oxide powder becomes slightly conductive when exposed to the ambient humidity level. The electrical insulation must be tested with $+250\ V$ DC voltage to verify if the resistance across the inner conductor and the shield of the cable is sufficiently high,

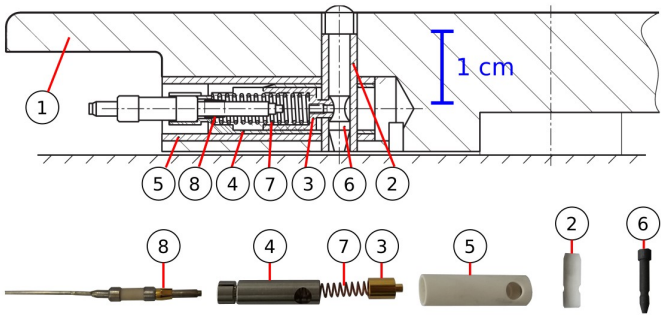

FIG. 2. Cross-sectional view of the probe assembly and photos of the individual components labeled: ① Graphite tile housing ② Vertical aluminum nitride electrical insulation tube ③ Gold coated copper beryllium finger electrical contact ④ Stainless steel housing for the cable inner conductor (end of the Thermocoax® cable) ⑤ Horizontal aluminum nitride electrical insulation tube ⑥ Graphite probe tip ⑦ Nickel based alloy spring and ⑧ Gold coated copper beryllium contactor (tiny ring mounted onto the cable inner conductor).

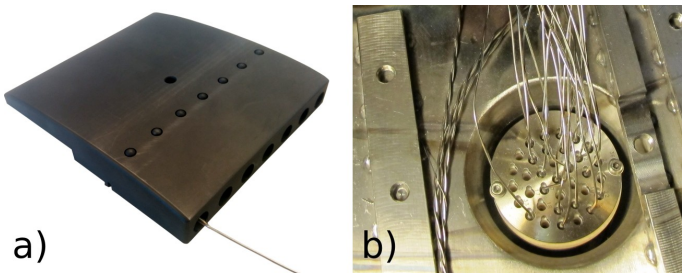

FIG. 3. Langmuir probe tile **a)** ready for installation with a single Thermocoax® cable connected to the first probe for illustration and vacuum feed-through **b)** seen from inside the tokamak vessel after the protective tiles have been removed.

i.e. at least 100 $M\Omega$.

The length of the Thermocoax® cables between probe tips and vacuum feedthroughs, see 3 **b)**, is typically $\approx 2m$. The vacuum feedthroughs are special units from the Kurt J. Lesker Company®. They are mounted on $DN63\ CF$ vacuum flanges. Each unit carries a maximum of 35 conductors. Electrical contact is provided by male pins embedded into the ceramic body of the feedthroughs and by specific female copper contactors that are brazed onto the inner conductor of the Thermocoax® cables.

The in-vessel transmission line is then followed with $\approx 20\ m$ of 19 twisted pairs Mueller® cables, connecting the vacuum feedthroughs with the Langmuir probe electronics cubicle. Each probe conductor from the vacuum feedthrough is connected to both conductors of each twisted pair in the Mueller® cable in order to minimize the line resistance. The advantage of twisted pairs is lost by using both conductors to carry the same signal but the high frequency properties are maintained thanks to the individual grounded screens wrapped around each pair. Each of the 19 pairs Mueller® cable carries a maximum of 19 signals.

The overall capacitances of the transmission lines have been measured directly at 10 kHz and 100 kHz and the values are found between $C_{line} = 3.5\ nF$ and $C_{line} = 6\ nF$ depending on the line. These measurements are consistent with measurements on spare Thermocoax® cables $C_{Thermocoax} = 0.61\ nFm^{-1}$ and on twisted pairs from spare Mueller® cables $C_{Mueller} = 0.19\ nFm^{-1}$.

The overall resistances and inductances of the entire lines have not been measured directly. Estimates are given here based on measurements done on spare cables:

- The overall resistance is estimated to be $R_{line} \approx 1.3\ \Omega$, given the measured DC resistance $\approx 0.5\ \Omega$ of the probe assembly shown in FIG. 2 connected to a 2 m long Thermocoax® cable and given the measured resistance per unit length of a twisted pair from the Mueller® cable $R_{Mueller} \approx 0.04\ \Omega m^{-1}$. In the scenario where nickel based alloy springs are taken into account as explained earlier, the overall resistance is estimated to be $R_{line} \approx 2.2\ \Omega$.

- The overall inductance of the line is estimated to be $L_{line} \approx 15.4\ \mu H$, given the measured inductance per unit length of the Thermocoax® cable $L_{Thermocoax} = 0.7\ \mu Hm^{-1}$ and the measured inductance per unit length of a twisted pair from the Mueller® cable $L_{Mueller} \approx 0.7\ \mu Hm^{-1}$ (measurements performed at 100 kHz).

Langmuir probe electronics are necessarily referenced to the vacuum vessel ground, as opposed to most diagnostics at TCV which are referenced to the TCV building ground. The electronics cubicles are therefore separated from the building ground using an isolation transformer.

The 19 pairs Mueller® cable shield connects the electronics cubicles to the vacuum vessel ground, as sketched in FIG. 4. The cables do not encircle the vacuum vessel to avoid receiving the loop voltage induced by the central solenoid.

During a discharge, the time derivative of the vertical magnetic field can be as high as $\approx 0.05\ T/s$ in the region between the vacuum vessel and the cubicles ($r \approx 2\ m$, $z \approx -1.5\ m$) mainly due to the contribution of poloidal field coils. The inductive current going through the shield can be estimated from the resistance $R_{shield} \approx 0.1\ \Omega$. The stray current can be approximated with the laws of Ohm and Faraday:

$$I = \frac{U}{R_{shield}} = \frac{S\frac{dB}{dt}}{R_{shield}} \approx \frac{10\ m^2 \cdot 0.05\ T/s}{0.1\ \Omega} \approx 5\ A \quad (1)$$

This relatively modest stray current is not expected to perturb the measurements or the TCV magnetic field.

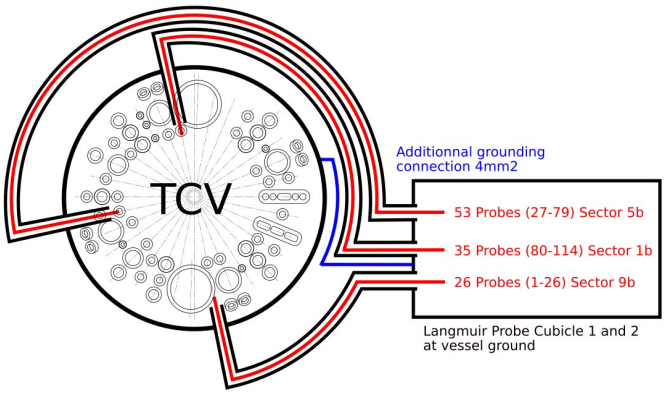

FIG. 4. Electrical connections in between the tokamak and the electronics cubicle with biased conductors in red and grounded conductors in black (top view).

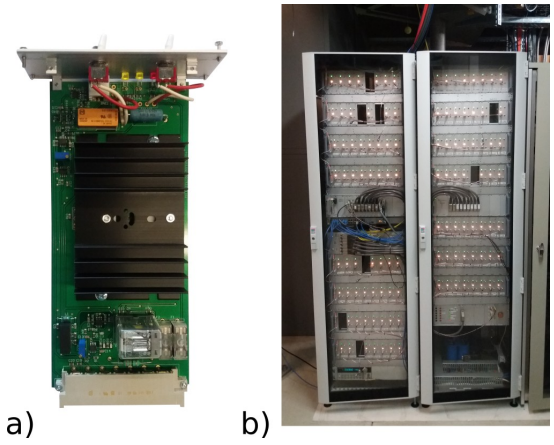

FIG. 5. Single amplifier **a)** and complete cubicle **b)**. Amplifiers have been removed where the in-vessel transmission line has been damaged.

III. DESIGN OF THE AMPLIFIER CIRCUITRY

There have been three different generations of Langmuir probe amplifiers developed at SPC. Only the third generation is described in detail in this paper. The first generation did not have any custom amplification module and was based on $PB58A$ APEX® amplifiers. In the second generation, the APEX® amplifier was replaced by a patch developed at SPC. The patch will not be described in this paper because it can be considered as obsolete when compared to the last generation. Indeed, the third generation features an improved current measurement and an improved current limitation system over the second generation.

This section is organized in five subsections. Sec. *III A* presents the general constraints given from plasma parameters while Sec. *III B*, Sec. *III C*, Sec. *III D* and Sec. *III E* cover, respectively, the choice of power supplies, the amplification system, the potential and current measurement system and the current limitation system.

A single amplifier module is shown in FIG 5, as well as the cubicle installed in the TCV basement level. The organization of the electronics of a single amplifier within the complete diagnostic environment is illustrated schematically in FIG 6 and a complete drawing of the circuitry is given in FIG 7.

Amplifiers, waveforms, acquisitions and power supplies are all referenced to the torus ground. Electrical insulation from the building ground is provided with optical fibers once the signal has been digitized, see FIG 6.

A. Requirements

On TCV, the following relation is assumed for the current flowing through the sheath and to the probe as a function of applied probe voltage [6]:

$$I_{pr} = I_{sat}\left[1 + \alpha(V_{pr} - V_{fl}) - e^{\frac{V_{pr}-V_{fl}}{T_e}}\right], \qquad (2)$$

where V_{fl} is the potential at which there is no net current drawn from the plasma, α is a coefficient taking into account the increase in the effective ion collection area with voltage in the ion saturation domain due to sheath expansion, T_e is the electron temperature expressed in eV and I_{sat} corresponds to the ion current drawn at $V_{pr} \leq V_{fl}$. In the case of probe tips with relatively small ion collection area, e.g. flush probes, the parameter α is mandatory for the interpretation of measurements. It is less critical in the case of domed probes.

The ion saturation current I_{sat} is given by the Bohm condition [4]:

$$I_{sat} = n_{e,se} e c_s S, \qquad (3)$$

where $n_{e,se}$ is the electron density at the entrance of the sheath, S is the effective ion collection area of the probe and c_s the Bohm velocity, given by [4]:

$$c_s = \sqrt{\frac{e(T_e + \gamma T_i)}{m_i}}, \qquad (4)$$

where e is the elementary charge, T_e and T_i are the electron and ion temperature expressed in eV, m_i is the ion mass, and γ is the adiabatic index. $\gamma = 1$ is chosen as a default value to assure compatibility with previous TCV studies [6]. It corresponds to the sound speed of an isothermal plasma. Since T_i is difficult to measure in the boundary plasma of tokamaks, the assumption that $T_i = T_e$ is usually made [6].

In order to measure the current-voltage characteristics described in EQ. (2), V_{pr} must be swept from a strongly negative voltage $V_- \approx V_{fl} - 3T_e$ to obtain sufficient saturation for the ion flow, up to the plasma potential $V_p \approx V_{fl} + 3T_e$ [4].

The floating potential is usually found in between $V_{fl} = -30\ V$ and $V_{fl} = +15\ V$ in TCV plasmas. Target electron temperatures typically do not exceed $T_e \approx 30\ eV$. Therefore the biased probe voltage should range at least from $V_{min} \approx -30\ V - 3 \cdot 30\ V = -120\ V$ up to $V_{max} = 15\ V + 3 \cdot 30\ V = 105\ V$. Two separated DC power supplies have been selected to provide the sufficient extrema voltages $V_{pr} = \pm 110\ V$. It should be noted, however, that for some discharges, the floating potential is extremely low and T_e above 30 eV, e.g $V_{fl} = -45\ V$ and $T_e = 45\ eV$ for shot #58182 (low density, high plasma current, high confinement mode discharge). In this particular case, the amplifiers are unable to apply a voltage low enough to fully approach ion saturation.

Target electron densities at the sheath edge typically do not exceed $n_{e,se} \approx 1.5 \cdot 10^{19}\ m^{-3}$. It is possible to obtain an estimate of the corresponding ion saturation current from EQ. 3 and 4:

$$I_{sat} = n_{e,se} e S \sqrt{\frac{e(T_e + \gamma T_i)}{m_i}} \approx 0.36\ A, \qquad (5)$$

with $n_{e,se} = 1.5 \cdot 10^{19}\ m^{-3}$, $S = 2.8\ mm^2$ the projected area of the domed probes used in TCV with incident field lines at grazing angle $\alpha = 0°$, $T_e = T_i = 30\ eV$, $m_i = 3.32 \cdot 10^{-27}\ kg$ in deuterium plasma and $\gamma = 1$. Therefore the $-110\ V$ power supply has been chosen to deliver 9 A DC, sufficient to provide the maximum current calculated in equation 5 to at least $9/0.36 \approx 25$ probes.

The electron saturation current with the same plasma parameters can be estimated as follows [4] [6]:

$$I_{sat,e} = -|I_{sat}| \cdot \sqrt{\frac{2m_i}{\pi m_e}\left(\frac{T_e}{T_e + \gamma T_i}\right)} \approx -12.3\ A. \qquad (6)$$

The theoretical ratio $|I_{sat,e}/I_{sat}| \approx 34$ is usually much higher than the experimental ratio of $I_{sat,e}/I_{sat} \approx 6$ [12] mainly because the electron depleted region in magnetized plasmas becomes longer than the mean free path of electron ion collisions [12] and the collisionless assumption required in sheath theory is no longer valid. Nevertheless, the estimated maximum electron saturation current $I_{sat,e} \approx 6 I_{sat} \approx 2.16\ A$ is found beyond the acquisition range limit $\pm 2\ A$ in experiments with high target temperature and density.

The positive $+110\ V$ DC power supply has been sized to deliver 18 A, enough to attain the 2 A acquisition limit in electron saturation simultaneously on 9 different probe tips.

B. Power supplies

The positive $+110\ V$ power supply consists of 2 Camtech® $HPV10001$ $9.1A$ units and the negative $-110\ V$ power supply consists of a single one. These units include galvanic insulation and can therefore be directly connected between the standard $220V$ AC network and the torus ground. Both positive and negative terminals are connected to large capacitances $C_{out} = 2800\ \mu F$. These large capacitances add up to the Camtech® power supplies internal capacitances in order to provide a current transiently exceeding $19A$ in the case of electron saturation with swept bias voltage.

The positive $+15V$ power supply consists of a $26A$ Camtech® $HSE04801$ and the negative $-15V$ supply consists of a $5A$ Camtech® $HSW00751$. The current requirement is larger for the positive voltage since it supplies current for the $\pm 15VF$ DC-DC power supply, item ④ in FIG. 8. The highest current drawn per amplifier is $\approx 55\ mA$ for the DC-DC power supply, as explained in Sec. $III\,E$. Therefore the $26A$ unit is sufficient to power hundreds of amplifiers at the same time.

A delay switch ensures that the $\pm 15V$ power supply is always activated once the ± 110 power supply turns on.

C. Amplification

The probe voltage is remotely controlled by changing the waveform generator settings. The waveform generator voltage is amplified 50 times with the overall negative feedback loop on the custom amplifier circuitry, see item ② in FIG. 7 and item ② in FIG. 8. The gain is precisely tuned on each amplifier by changing the resistance of the 500 Ω potentiometer.

A $2.2\ nF$ capacitance has been set on the negative feedback loop of the first OP-Amp, see item ① in FIG. 8. This capacitance primarily determines the measured cutoff frequency of the overall amplifier $f_{cutoff} \approx 25\ kHz$ for stability purposes. The cutoff frequency is much higher than the typical sweeping frequency necessary for time-averaged measurements $f_{sweep} \approx 300\ Hz$. However, it does not allow the ultra fast sweeping required to resolve fluctuations from plasma micro-turbulence [13].

The second OP-Amp, see item ③ in FIG. 8, is a so-called *suspended OP-Amp*: the potential reference VF of the positive and negative power supplies $VF \pm 15\ V$ is very close to the probe voltage, therefore suppressing the need for any large potential differences at the OP-Amp terminals.

D. Potential and current measurement system

The voltage measurement consists in dividing the probe voltage by a factor of 15 before the analog-to-digital conversion with a resistive divider. The OP-Amp $OP42GS$, item ⑦ in FIG. 7 is connected as a voltage follower and the resistances are selected in order to obtain $\pm 10\ V$ at the digitizer when the probe voltage is $\pm 150\ V$. The acquisition is provided by D-TACQ Solutions Ltd® ACQ196CPCI 16 bits digitizers sampling at $200kS/s$. The voltage measurement range is sufficient to cover the power supply range $\pm 110\ V$. Probe voltages

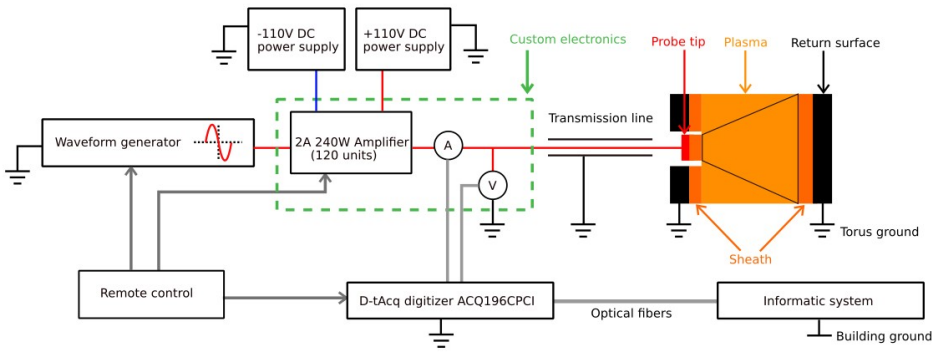

FIG. 6. Diagram including the main components of the electronic system and the equivalent circuit for the Langmuir probe with the current flowing between the probe tip and a larger return surface.

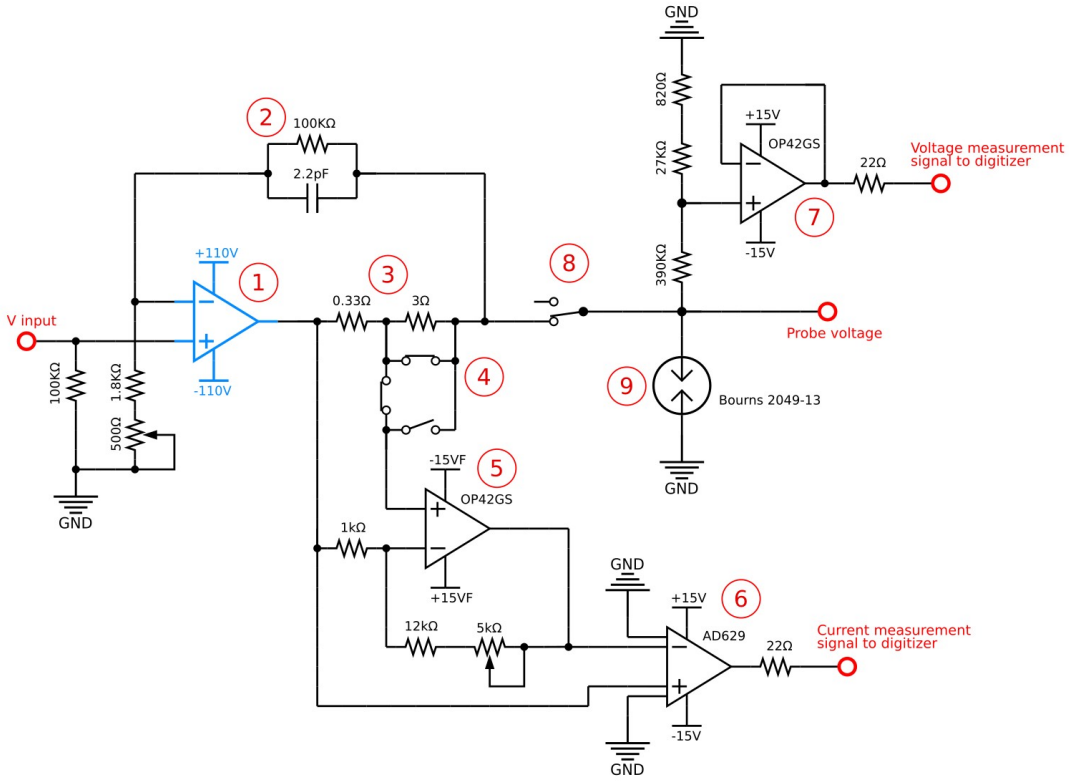

FIG. 7. Custom Langmuir probe electronics: ① Custom amplifier in blue (see FIG. 8), ② Overall negative feedback loop, ③ Shunt resistors, ④ Shunt relays (here the 3 Ω resistor is bypassed to select the large current measurements $\pm 2A$), ⑤ OP-Amp used to amplify the current measurement signal (the potential drop across the shunt resistors), ⑥ High common mode unity gain OP-Amp referencing to ground the current measurement signal, ⑦ OP-Amp used as a voltage divider for the potential measurement, ⑧ Switch to select either the biased probe potential mode V_{pr} or the floating potential mode V_{fl} and ⑨ Surge protection.

beyond $\pm 150\ V$ are obtained only in the non-stationary case of plasma disruptions with the probes in V_{fl} mode.

The current measurement system is more complex than the voltage measurement one. In the first generation of amplifiers, the voltage drop across the shunt resistors was directly sent to the differential inputs of a high common mode unity gain OP-Amp. The voltage drop range is $\pm 0.66\ V$ and it was then amplified to match the digitizer input voltage range $\pm 10\ V$. Virtual currents originating from the imperfect common mode rejection were acquired, as shown in FIG. 9. These residual currents have to be subtracted from the data by averaging the traces

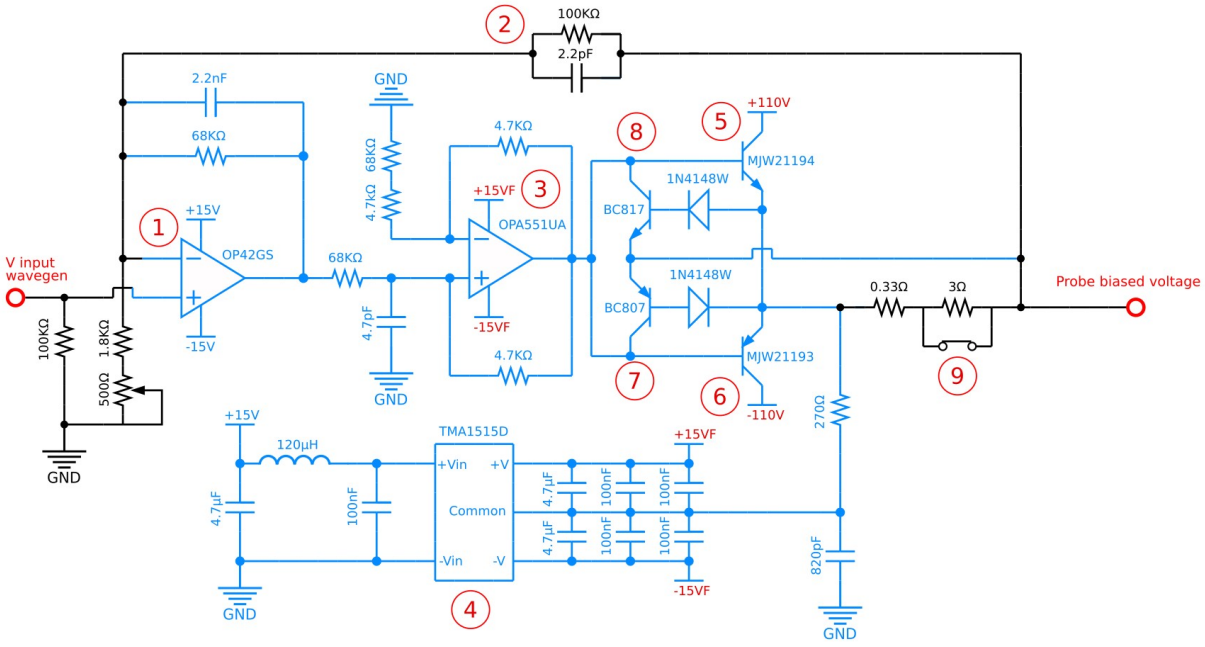

FIG. 8. Detailed circuit of the custom amplifier (item ① in FIG. 7): ① First OP-Amp ② Overall negative feedback loop from probe voltage, ③ Second OP-Amp used to step up the voltage ④ DC-DC power supply for the second OP-Amp with the "common" reference being close to the probe potential, ⑤ Silicon power transistor delivering the negative current, ⑥ Silicon power transistor delivering the positive current, ⑦ Transistor used to limit the negative current, ⑧ Transistor used to limit the positive current and ⑨ Shunt relays (here the 3Ω resistor is bypassed to select the large current measurements $\pm 2A$).

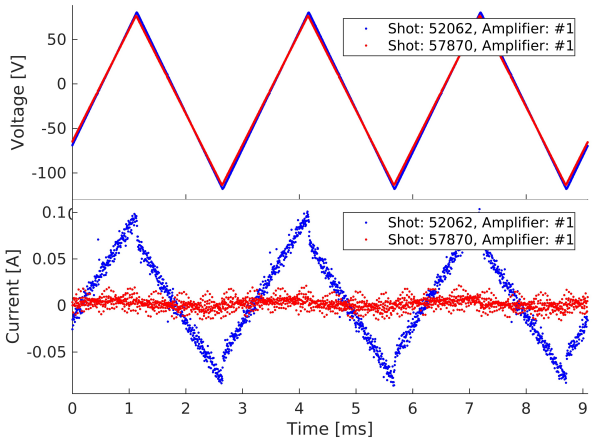

FIG. 9. Current measurement during a triangular voltage sweep from the first generation of amplifier in shot #52062 and from the third generation amplifier in shot #57870. Virtual/capacitive current are recorded after the end of the plasma discharge.

before or after the plasma discharge. OP-Amps $AD629$ have also been used in other Langmuir probe systems in a similar fashion in order to address the issue of common mode rejection [14].

In the third generation of amplifiers, the potential drop through the shunt resistors is first amplified with an OP-Amp, see item ⑤ in FIG. 7. The signal is then referenced to ground potential through the high common mode unity gain OP-Amp $AD629$ in order to be acquired, see item ⑥ in FIG. 7. Virtual currents have been highly reduced thanks to the higher signal to common-mode ratio, as seen in FIG. 9. The subtraction of virtual currents is still maintained in the routines for the Langmuir probe analysis [6] because capacitive currents are still present with the new electronics.

The current measurement is calibrated in order to obtain $\pm 10\ V$ at the digitizer when the current is $\pm 0.2\ A$ in low current mode and $\pm 2\ A$ in high current mode. Dense and hot plasma at the probe can regularly attain the $2\ A$ acquisition limit in electron saturation. The saturation of the acquisition does not represent any significant information loss since data points in the electron saturation region are not taken into account by the minimum temperature method chosen for the 4 parameters fit of the IV curve [6] given in equation 2.

In the case of negative bias and when the shunt selection for large current $\pm 2\ A$ is chosen, the current limitation is always above the probe current, which is typically $I_{sat} < 0.36\ A$, see equation (5).

The measured resonance frequency point of the current measurement system is $f_{res} \approx 250\ kHz$. Therefore any current fluctuation faster than the upper cut-off fre-

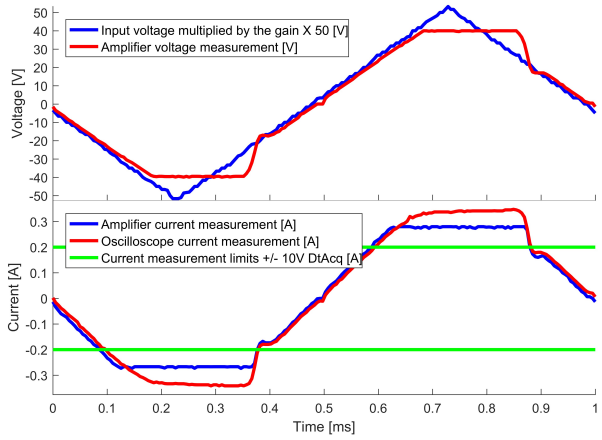

FIG. 10. Current limitation test with a 1 kHz triangular voltage sweep, 100 Ω load and the shunt selection for small current measurements ±0.2 A.

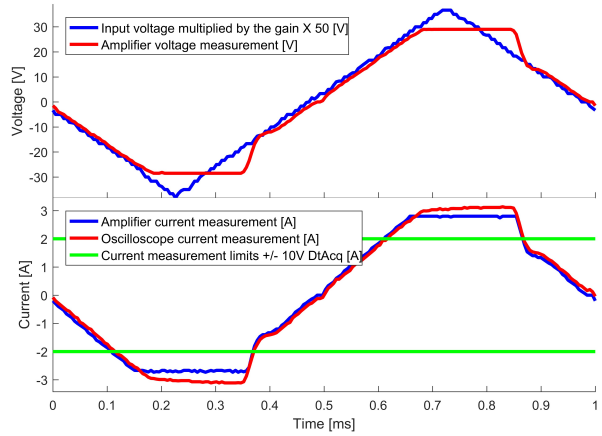

FIG. 11. Current limitation test with a 1 kHz triangular voltage sweep, 10 Ω load and the shunt selection for large current measurements ±2 A.

quency $f_{cm} \approx f_{res}$ can not be seen in the acquired data.

E. Current limitation system

Current limitation is necessary to avoid over-currents in the silicon power transistors, to limit heat-flux onto the probe tips (in the electron saturation region) and to avoid the current starvation of the high voltage power supplies ±110 V which can happen when many probes draw high currents at the same time.

The current limits are determined by the sum of the diode threshold voltages from the transistors $BC817$ and $BC807$, see items ⑦ and ⑧ in FIG. 8, and from the 2 diodes $1N4148W$. Once the voltage drop across the shunt resistors overcomes the sum of the diode threshold voltages $V_{threshold} \approx 0.6\ V + 0.6\ V \approx 3.33\ \Omega \cdot 0.35\ A$ or $0.33\ \Omega \cdot 3.5\ A$, the OP-Amp $OPA551UA$ delivers current directly to the Langmuir probe and the silicon power transistor is bypassed. The large current requested by the overall feedback loop can rapidly damage the OP-Amp $OPA551UA$. This is why a 270 Ω resistor has been installed to starve the floating power supply of the OP-Amp $OPA551UA$ once the return current becomes larger than $I_{max} \approx \frac{15\ V}{270\ \Omega} \approx 55\ mA$. Therefore, even though the voltage required by the overall feedback, item ② in FIG. 8, is still very high, the effective voltage at the OP-Amp $OPA551UA$ output and the probe voltage are lower, just enough to supply the current limit $\pm 0.35\ A / \pm 3.5\ A$.

Tests of the current limitation system are presented in FIG. 10 for the ±0.2 A shunt mode and in FIG. 11 for the 2 A shunt mode. A specific setup with a voltage isolator device connected to an oscilloscope referenced to ground is required to measure the actual current limit. Indeed, the maximum current measurable by the amplifier circuitry is lower than its actual current limitation $\approx \pm 0.35\ A / \pm 3.5\ A$, due to the finite voltage $VF \pm 15\ V$ supplying the OP-amp $AD629$, item ⑥ in FIG. 7. The test frequency $f = 1000\ Hz$ is chosen to be similar to the typical sweeping frequency used at TCV. The test peak voltages and the test resistors 10 Ω and 100 Ω have been chosen in order to attain the current limit.

The probe current is limited to $I_{pr} \approx \pm 0.35\ A$ as shown in FIG. 10 when both shunt resistors are connected. It is limited to $I_{pr} \approx \pm 3.5\ A$ when the 3 Ω shunt resistor is bypassed as shown in FIG. 11. The ±0.27 A and ±2.7 A plateaus observed with an oscilloscope for the amplifier current measurement, plotted in blue in the bottom panels of FIG. 10 and FIG. 11, correspond to the saturation of the high common mode OP-Amp due to the finite voltage supply ±15 V. The measurement would have been limited to ±10 V if the measurement had been done with the digitizers instead of an oscilloscope, as explained in Sec. $III\ D$.

IV. PROTECTION AGAINST AMPLIFIER DAMAGE

The silicon power transistors, items ⑤ and ⑥ in FIG. 8, are the most frequent components responsible for amplification failure. Usually both components are damaged at the same time. This may lead to a short circuit between the power supply terminals ±110V which is rapidly stopped by 2A fuses installed in series with the power supply terminals of each amplifier. The transistors for the current limitation, items ⑦ and ⑧ in FIG. 8, are also damaged in ≈ 20% of the cases. The typical rate of failure is one amplifier per week of probe operation at TCV with the loss of 29 amplifiers between July 2017 and April 2018.

These failures can be caused by current surges faster than the time response of the current limitation system

described in Sec. *III E*. It can be also caused by absorption of energy when the plasma itself transiently acts as a power supply instead of a load. The power transistors are indeed vulnerable to non-standard operation such as base-emitter junction breakdown in this case.

These processes mostly occur during transient plasma events such as: tokamak plasma current disruptions, Edge Localized Mode (ELM) transients and electron cyclotron microwave power not absorbed by the plasma. The corresponding timescales of these processes are $\approx 0.5\ ms$ and $\approx 1\ ms$ (typical durations of the plasma thermal quench and the plasma current quench), $\approx 0.5\ ms$ (ELMs) and $\approx 1\ s$ (microwave power).

The lack of effectiveness of fuse protection in TCV is discussed in *IV A*. An unsuccessful attempt to prevent amplifier damage with over-voltage surge protectors is described in *IV B*. The possibility of adding extra inductances to limit fast current peaks is described in *IV C*. Finally, another possible solution to avoid amplifier damage by decreasing the effective capacitance of the power supply is described in *IV D*.

A. Attempt to prevent amplifier damage with fuses

Cartridge fuses FSF5X20250V2A (reference 0034.1519) were used in series with the transmission line on the first generation of amplifiers. Due to the inefficiency of these fuses, it was decided to eliminate them in the latest generation.

The lack of fuse effectiveness is believed to be linked to the fuse breaking time. Even if the current is large enough to provide the integrated energy $RI^2\Delta t$ necessary to melt the conductor, at least a few milliseconds are required for any fuse to completely stop the current [15] due to the formation of an electrical arc. Therefore the fuse would not protect the transistors during the first $\Delta t = 1\ ms$ of any off-normal events, regardless of the current value.

B. Attempt to prevent amplifier damage with surge protectors

The main purpose of using surge protectors is to prevent the probe potential from exceeding the power supply range $\pm 110\ V$.

Surge protectors, as well as varistors [16] fulfill protection requirements because of their fast time response (ranging from $\approx 50\ ns$ to $10\ \mu s$ depending on the product). Surge protectors Bourns® 2049 – 13 with the specified DC sparkover $130\ V$ were connected directly in between the transmission line conductor and ground, see item ⑨ in FIG. 7. Once the voltage difference between the grounded electrode and the electrode at probe voltage is higher than the surge protector breakdown voltage, a Paschen discharge is initiated in the low pressure gas chamber to short-circuit the transmission line. The surge protector breakdown was tested in the laboratory, as described in *IV B 1* and surge protectors were then installed in the machine to evaluate the protection effectiveness, as described in *IV B 2*.

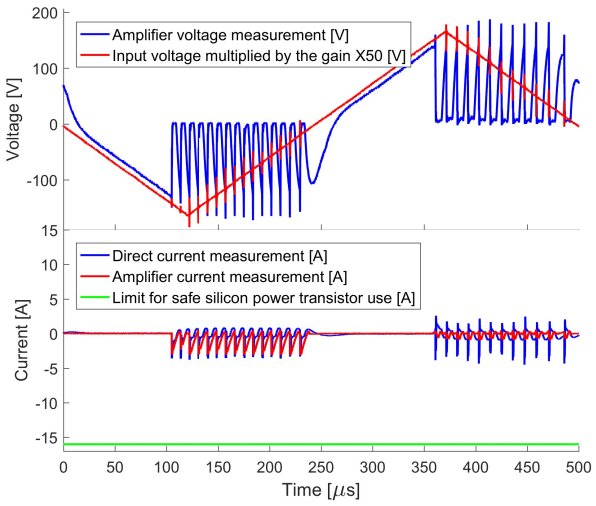

FIG. 12. Time traces of the surge protection being switched on with a triangular waveform at $2\ kHz$. Each sawtooth oscillation consists of three different phases: the discharge time, a glow period and the voltage ramp-up time of the amplifier.

1. Testing surge protectors before installation at TCV

A test has been done without any resistive load at the amplifier output in order to see the bare surge protector current. Once the surge protector is triggered, current and voltage show a characteristic sawtooth behavior oscillating at $\approx 100\ kHz$ as shown in FIG. 12. The maximum current rating $I_{collector} = 16\ A$ according to the manufacturer for the silicon power transistors has been plotted on the same figure. All of the current signals shown in FIG. 12 corresponds to the current flowing through the surge protector. The $\approx 10\ \mu s$ period of this sawtooth oscillation is the sum of the measured breakdown time $t_{breakdown} \approx 1\ \mu s$, a glow period $t_{glow} \approx 4\ \mu s$ and the voltage ramp up time constant $t_{ramp} \approx 5\ \mu s$. Once triggered, surge protectors switch off again once the voltage applied is reversed. Therefore it assures reliable data acquisition $0.75\ ms$ after any event that could have triggered the surge protector (1/4 of the typical triangular waveform sweeping period applied).

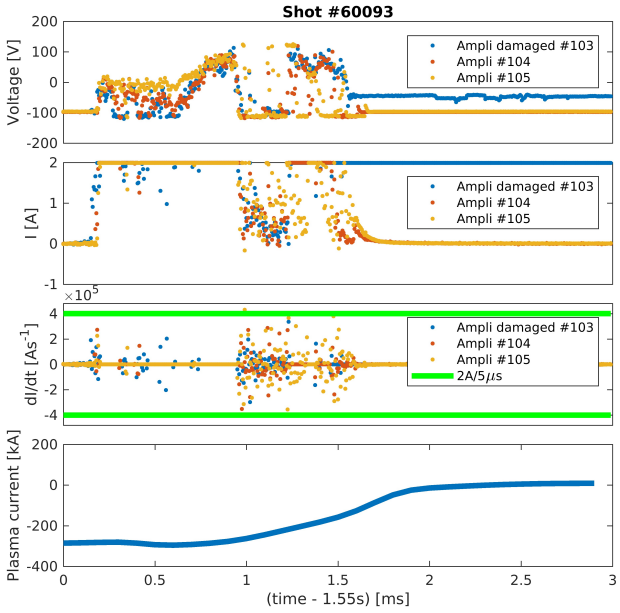

FIG. 13. Time traces during a disruption where the amplifier connected to the probe #103 is damaged. For comparison, time traces of neighboring amplifiers are also shown.

2. Installation of surge protectors at TCV and unsuccessful protection

The installation of surge protectors on 30 amplifiers out of 114 did not decrease the failure rate. From March 2018 to July 2018, 3 out of the 13 damaged amplifiers were equipped with surge protectors. The surge protectors on the damaged amplifiers did not show any sign of fatigue. For one of these damaged amplifiers, the time traces of the event were recorded in the experiment #60093, as shown in FIG. 13. On this figure, it can be seen that after the disruption, the amplifier #103 is no longer able to provide the $-100\ V$ voltage required for I_{sat} measurement, proving that the silicon power transistor lost its semiconductor properties. It is interesting to notice that the time derivatives of the current are very high, sometimes exceeding $2\ A/5\ \mu s$ (the positive acquisition limit divided by the acquisition period).

The lesson learned is that amplifier failure can happen within the voltage range from the power supplies $\pm 110\ V$ and therefore surge protectors do not offer an adequate protection.

C. Preventing amplifier damage by increasing the transmission line inductance

In order to limit the peak current flowing before the current limitation system has time to trigger, a simple solution is to increase the inductance of the transmission line. Any sudden current change would change the probe voltage in order to oppose the increase in current following the equation $U_L = -LdI/dt$. The second positive effect would be to stabilize the emitter and collector voltages of the transistor in order to avoid the emitter voltage to transiently surpass the base voltage.

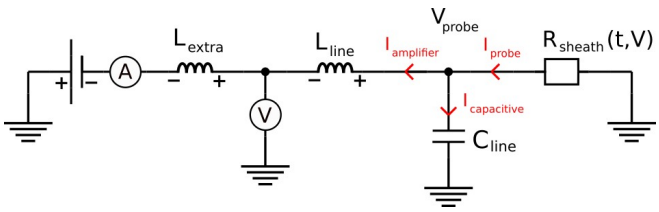

FIG. 14. Equivalent RLC circuit for the Langmuir probe taking into account the inductance and the capacitance of the transmission line and an extra inductance. Here $I_{amplifier} > 0$ and $dI_{amplifier}/dt > 0$ were assumed, such that the inductive voltages are counteracting the amplifier voltage.

In the following sections, some explanations and calculations are presented in order to describe the protection mechanism and to justify the choice of the proper inductance value required for protection.

1. RLC equivalent circuit and measurement considerations

The transmission line can be modeled as a single RLC circuit because, at the cutoff frequency of the amplifier current measurement $f_{cm} \approx 250\ kHz$, the wavelength of any fluctuation is much longer than the transmission line length $\approx 20\ m$:

$$\lambda = \frac{c_{Mueller}}{f} = \frac{1}{f_{cm}\sqrt{L_{Mueller}C_{Mueller}}} \approx 350\ m, \quad (7)$$

where $c_{Mueller}$ is the speed of light in the 19 pairs Mueller® cable, $f_{cm} = 250\ kHz$ the cutoff frequency from the amplifier current measurement, $L_{Mueller} \approx 0.7\ \mu Hm^{-1}$ the inductance per unit length and $C_{Mueller} \approx 0.19\ nFm^{-1}$ the capacitance per unit length of the 19 pairs Mueller® cable. The $250\ kHz$ frequency is relevant to consider because most of the plasma fluctuation power was found below $\approx 250\ kHz$ at TCV in 2004 with the former fast probe sampling I_{sat} and V_{fl} at $6\ MHz$ [17].

The resistance in the RLC circuit is the sheath resistance $R_{sheath}(t, V)$, a function dependent on both time and probe voltage. The equivalent circuit is represented in FIG. 14. The extra inductance should be mounted in series with the transmission line and behind the voltage measurement, in order to take into account the inductive voltage in the measurement of the probe voltage. In any case, inductive voltages can be deduced from the time derivative of current measurements.

2. Determination of the minimum inductance value required

For effective protection, the voltage drop across the inductance should be of the order of a few times T_e. Current surges above the rating of the silicon power transistors of $I = 16\ A$ must be inhibited for the reaction time of $\approx 5\ \mu s$ of the current limitation system.

Taking a desired voltage drop across the inductance $U = 100\ V$, the required total inductance of the line can be determined:

$$L = |-\frac{U}{dI/dt}| = \frac{100\ V}{16/(5\cdot 10^{-6})\ As^{-1}} \approx 31\ \mu H. \quad (8)$$

This value is higher than the inductance of the transmission lines currently installed at TCV, $L_{line} \approx 15.4\ \mu H$, and therefore an additional $L_{extra} > 15\ \mu H$ would be required. It must be noted that capacitive currents do not play any significant role during large transient events. Indeed a simple calculation shows that these currents are negligible when compared to the probe current:

$$I_C = C_{line}\frac{dV}{dt} \approx 5\cdot 10^{-9}\ F \cdot \frac{100\ V}{5\cdot 10^{-6}\ s} = 0.1\ A \quad (9)$$

3. Determination of the maximum tolerable inductance value

In principle, the extra inductance does not affect the current-voltage measurements because the voltage is measured on the probe-side of L_{extra}. The voltage drops between the measurement location and the probe tips across L_{line} and capacitive currents due to C_{line} can in principle be corrected for.

However, it is important to ensure that the probe voltage stays well in the ion saturation regime at all times when operating the probes in I_{sat} mode (probe current I_{pr} recorded as a function of time rather than as a function of probe voltage V_{pr}). Thus, the probe voltage should not deviate considerably from $V_{pr} \approx -110\ V$ at any time. FIG. 15. shows the expected inductive voltages for different values of L_{extra} and for an experimental probe signal with relatively high current fluctuation levels. This shows that inductive voltages are $< \pm 1\ V (< \pm\ 2V)$ for $L_{extra} = 30\ \mu H$ ($L_{extra} = 60\ \mu H$) at any time. Therefore, $L_{extra} = 30\ \mu H$ or even $L_{extra} = 60\ \mu H$ would be tolerable.

Inductive voltages fluctuating with time will cause capacitive currents. However, the calculated capacitive currents $I_C = C_{line}\cdot dU_L/dt$ with $L_{extra} = 30\ \mu H$ are found below 1.5 mA for the same data as in FIG. 15, which is acceptably low when compared to the time averaged ion saturation current in this experiment $I_{sat} \approx 0.22\ A$. Capacitive currents are expected to be the largest if the RLC circuit is excited by the time changing sheath resistance at the resonant frequency for LC circuits:

$$f_{res,LC} = \frac{1}{2\pi\sqrt{L_{line}\cdot C_{line}}} \approx 574\ kHz, \quad (10)$$

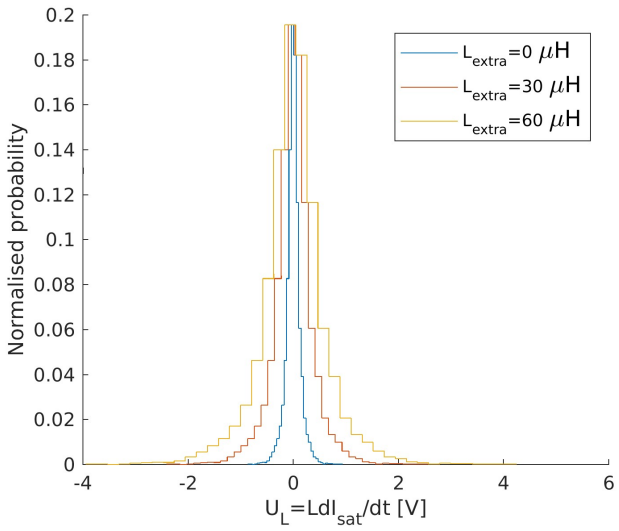

FIG. 15. Histograms of calculated inductive voltage in ion saturation ($V_{pr} < -90\ V$) from the standard shot #61273. Three different inductance values are taken for comparison. The data comes from the probe #6 ($t = 0.8\ s$ to $t = 1.1\ s$). This probe was specifically chosen because it was found to have the highest level of fluctuation as compared to other probes.

where $L_{line} = 15.4\ \mu H$ and $C_{line} = 5\ nF$. Increasing the line inductance by adding $L_{extra} = 30\ \mu H$ would result in lowering the resonant frequency down to $\approx 336\ kHz$. Since most of the plasma fluctuation power has been found below $\approx 250\ kHz$ [17], the risk of measuring large capacitive currents due to the LC resonance is relatively low.

To conclude, $L_{extra} = 30\ \mu H$ could be an appropriate inductance for effective protection against fast current surges ($< 5\mu s$) and negligible perturbation to the measurement.

D. Preventing amplifier damage by decreasing the effective power supply capacitance

The large capacitor mounted in parallel with the high voltage supply of each amplifier is a disadvantage during plasma transient events because it can provide large amounts of energy to the individual probe tips having the smallest sheath resistances. The issue can be partially solved by adding a resistor in series with the amplifier, see FIG. 16, in order to drop the line voltage in case of high current excursions.

For instance, in the presence of a $20A$ surge during a disruption when the bias voltage is $+100\ V$, the effective sheath resistance is $R_{sheath} = 100V/20A = 5\ \Omega$. In this case an additional resistance $R_{extra} = 10\ \Omega$ would lower the current down to $I = U/R = 100V/(5\Omega + 10\Omega) \approx 6.7A$. This reduction in current would likely be sufficient

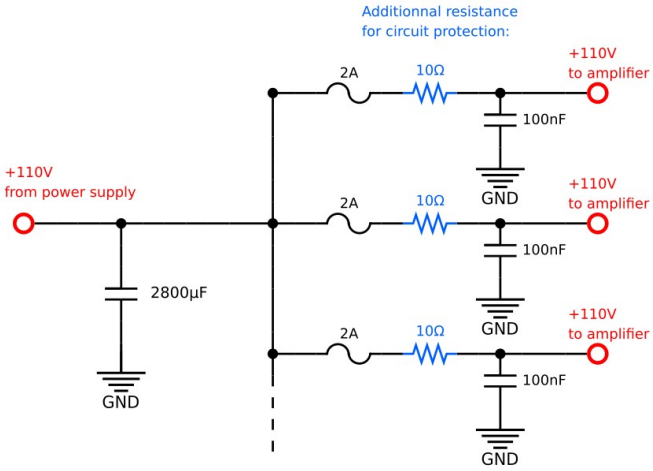

FIG. 16. Equivalent circuit for the positive $+110V$ power supply. All of the 120 amplifiers in the cubicles 1 and 2 are connected to the same capacitor. The same circuit applies for the negative $-110V$ power supply. The additional protective resistances R_{extra} are highlighted in blue.

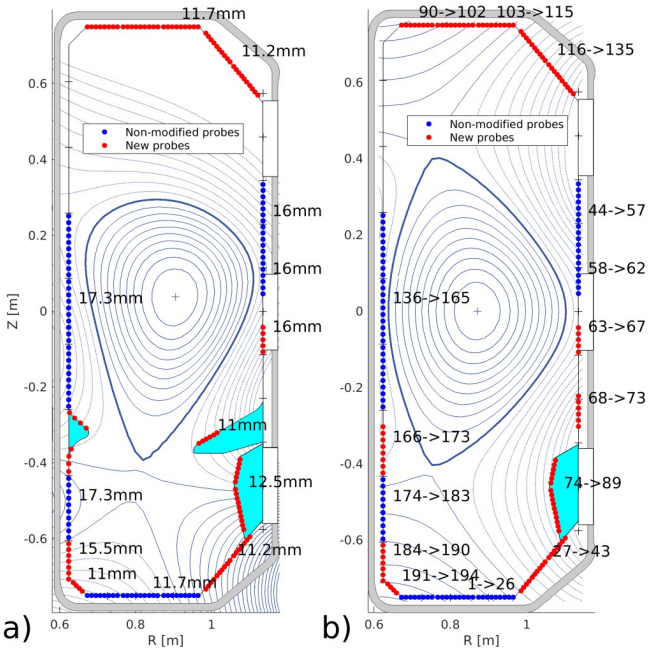

FIG. 17. Detail of the Langmuir probe array positions planned for the upgrade. The average distance in between probe tips is displayed for the upgrade with the first version of the baffles [20] to be installed in 2019 in **a)** and the probe numbering is shown for the upgrade without baffles in **b)**.

to prevent transistor damage.

During normal operation, the current can attain $2A$ in electron saturation. In this case the voltage of the power supply would be lowered down to $V = 110V - R_{extra}I = 110V - 2A \cdot 10\Omega = 90V$. The voltage drop would be acceptable from a physics point of view because most of the voltage range in the IV curve would remain accessible.

Circuit safety is always maintained when the voltage command is higher than the power supply voltage at the amplifier. Indeed, the floating power supply voltage $\pm 15VF$ of the second amplification OP-Amp, item ③ in FIG. 8, will drop through the 270Ω resistor and therefore limits its current.

The resistance protection solution is thought to be more effective than the inductance protection solution at the time of writing because it could address the problem of current surges regardless of the temporal characteristics. Installation is envisaged on some amplifiers to test the solution.

V. FUTURE EXTENDED PROBE COVERAGE

The first step of the ongoing divertor upgrade for the TCV tokamak features the installation of an in-vessel structure to form a divertor chamber and enhanced diagnostic capabilities [9]. New Langmuir probes will be installed to extend the coverage in order to be compatible with alternative divertor configurations [18] [19] such as single null with large flux expansion, double null, super-X and snowflake plasmas. The planned probe coverage in the poloidal plane is shown in FIG. 17 for both baffled and non-baffled operation. The electrical connection of the new cubicle is located on the other side of the tokamak building, see FIG. 18. Once again, the shield of the transmission lines will be continuous from the cubicles to the vacuum vessel.

VI. CONCLUSION AND SUMMARY

This paper has presented the electronics upgrade for the wall-embedded Langmuir probes on the TCV tokamak. The total number of amplifiers has been increased from 48 to 228, which allows all the probes to be operated simultaneously, greatly improving the flexibility of the measurement. The amplifiers are based on an inexpensive circuitry developed at the Swiss Plasma Center.

Details of the new amplifier circuitry have been described, with an emphasis on the amplification system, on the current limitation system, and on the voltage and current measurement system. Different possible solutions have been explored to prevent amplifier damage, which sometimes occurs due to electrical stresses from transient events during the TCV plasmas. It is concluded that the best solution comprises the addition of an extra resistor between the power supplies and the amplifiers. This solution will be tested in future experimental campaigns. Finally, the future extended Langmuir probe coverage has been introduced, which is one of the many TCV di-

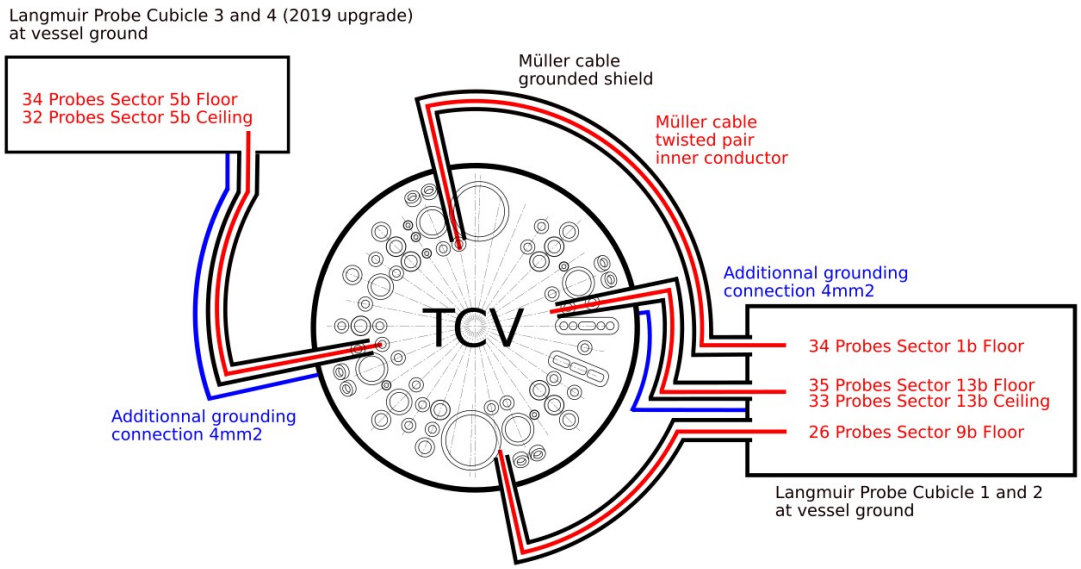

FIG. 18. Electrical connections in between the tokamak, the existing and planned electronics cubicles for the divertor upgrade with biased conductors in red and grounded conductors in black.

vertor upgrades under development and fabrication, and which will substantially improve the diagnostic coverage for a range of magnetic geometries, such as double-null, super-X and Snowflake plasmas.

ACKNOWLEDGMENTS

This work has been carried out within the framework of the EUROfusion Consortium and has received funding from the Euratom research and training program 2014 - 2018 and 2019 - 2020 under grant agreement No 633053. The views and opinions expressed herein do not necessarily reflect those of the European Commission or of the ITER Organization. This work was supported in part by the Swiss National Science Foundation.

[1]F. Hofmann, J. B. Lister, W. Anton, S. Barry, R. Behn, S. Bernel, G. Besson, F. Buhlmann, R. Chavan, M. Corboz, M. J. Dutch, B. P. Duval, D. Fasel, A. Favre, S. Franke, A. Heym, A. Hirt, C. Hollenstein, P. Isoz, B. Joye, X. Llobet, J. C. Magnin, B. Marletaz, P. Marmillod, Y. Martin, J. M. Mayor, J. M. Moret, C. Nieswand, P. J. Paris, A. Perez, Z. A. Pietrzyk, R. A. Pitts, A. Pochelon, R. Rage, O. Sauter, G. Tonetti, M. Q. Tran, F. Troyon, D. J. Ward, and H. Weisen, Plasma Physics and Controlled Fusion **36**, B277 (1994).

[2]S. Coda, J. Ahn, R. Albanese, S. Alberti, E. Alessi, S. Allan, H. Anand, G. Anastassiou, Y. Andrèbe, C. Angioni, M. Ariola, M. Bernert, M. Beurskens, W. Bin, P. Blanchard, T. C. Blanken, J. A. Boedo, T. Bolzonella, F. Bouquey, F. H. Braunmüller, H. Bufferand, P. Buratti, G. Calabró, Y. Camenen, D. Carnevale, F. Carpanese, F. Causa, R. Cesario, I. T. Chapman, O. Chellai, D. Choi, C. Cianfarani, G. Ciraolo, J. Citrin, S. Costea, F. Crisanti, N. Cruz, A. Czarnecka, J. Decker, G. De Masi, G. De Tommasi, D. Douai, M. Dunne, B. P. Duval, T. Eich, S. Elmore, B. Esposito, M. Faitsch, A. Fasoli, N. Fedorczak, F. Felici, O. Février, O. Ficker, S. Fietz, M. Fontana, L. Frassinetti, I. Furno, S. Galeani, A. Gallo, C. Galperti, S. Garavaglia, I. Garrido, B. Geiger, E. Giovannozzi, M. Gobbin, T. P. Goodman, G. Gorini, M. Gospodarczyk, G. Granucci, J. P. Graves, R. Guirlet, A. Hakola, C. Ham, J. Harrison, J. Hawke, P. Hennequin, B. Hnat, D. Hogeweij, J.-P. Hogge, C. Honoré, C. Hopf, J. Horáček, Z. Huang, V. Igochine, P. Innocente, C. Ionita Schrittwieser, H. Isliker, R. Jacquier, A. Jardin, J. Kamleitner, A. Karpushov, D. L. Keeling, N. Kirneva, M. Kong, M. Koubiti, J. Kovacic, A. Krämer-Flecken, N. Krawczyk, O. Kudlacek, B. Labit, E. Lazzaro, H. B. Le, B. Lipschultz, X. Llobet, B. Lomanowski, V. P. Loschiavo, T. Lunt, P. Maget, E. Maljaars, A. Malygin, M. Maraschek, C. Marini, P. Martin, Y. Martin, S. Mastrostefano, R. Maurizio, M. Mavridis, D. Mazon, R. McAdams, R. McDermott, A. Merle, H. Meyer, F. Militello, I. G. Miron, P. A. Molina Cabrera, J.-M. Moret, A. Moro, D. Moulton, V. Naulin, F. Nespoli, A. H. Nielsen, M. Nocente, R. Nouailletas, S. Nowak, T. Odstrčil, G. Papp, R. Papřok, A. Pau, G. Pautasso, V. Pericoli Ridolfini, P. Piovesan, C. Piron, T. Pisokas, L. Porte, M. Preynas, G. Ramogida, C. Rapson, J. J. Rasmussen, M. Reich, H. Reimerdes, C. Reux, P. Ricci, D. Rittich, F. Riva, T. Robinson, S. Saarelma, F. Saint-Laurent, O. Sauter, R. Scannell, C. Schlatter, B. Schneider, P. Schneider, R. Schrittwieser, F. Sciortino, M. Sertoli, U. Sheikh, B. Sieglin, M. Silva, J. Sinha, C. Sozzi, M. Spolaore, T. Stange, T. Stoltzfus-Dueck, P. Tamain, A. Teplukhina, D. Testa, C. Theiler, A. Thornton, L. Tophøj, M. Q. Tran, C. Tsironis, C. Tsui, A. Uccello, S. Vartanian, G. Verdoolaege, K. Verhaegh, L. Vermare, N. Vianello, W. A. J. Vijvers, L. Vlahos, N. M. T. Vu, N. Walkden, T. Wauters, H. Weisen, M. Wischmeier, P. Zestanakis, M. Zuin, and the EUROfusion MST1 Team, Nuclear Fusion **57**, 102011 (2017).

[3]H. M. Mott-Smith and I. Langmuir, Physical Review **28**, 727 (1926).

[4]P. C. Stangeby, *The Plasma Boundary of Magnetic Fusion De-*

vices, Series in Plasma Physics and Fluid Dynamics (Taylor and Francis, 2000).
[5]I. H. Hutchinson, *Principles of Plasma Diagnostics* (Cambridge University Press, 2005).
[6]O. Février, C. Theiler, H. De Oliveira, B. Labit, N. Fedorczak, and A. Baillod, Review of Scientific Instruments **89**, 053502 (2018).
[7]C. K. Tsui, J. A. Boedo, P. C. Stangeby, and TCV Team, Review of Scientific Instruments **89**, 013505 (2018).
[8]A. Fasoli and TCV Team, Nuclear Fusion **55**, 043006 (2015).
[9]H. Reimerdes, S. Alberti, P. Blanchard, P. Bruzzone, R. Chavan, S. Coda, B. P. Duval, A. Fasoli, B. Labit, B. Lipschultz, T. Lunt, Y. Martin, J. M. Moret, U. Sheikh, B. Sudki, D. Testa, C. Theiler, M. Toussaint, D. Uglietti, N. Vianello, and M. Wischmeier, Nuclear Materials And Energy **12**, 6. 1106 (2017).
[10]R. Chavan, R. Pitts, F. Hofmann, C. Hollenstein, J.-M. Moret, R. Rage, and G. Tonetti, Proceedings of the 17th Symposium on Fusion Technology, Rome, Italy, 14 - 18 September , 222 (1992).
[11]R. A. Pitts, S. Alberti, P. Blanchard, J. Horacek, H. Reimerdes, and P. C. Stangeby, Nuclear Fusion **43**, 1145 (2003).
[12]R. A. Pitts and P. C. Stangeby, Plasma Physics and Controlled Fusion **32**, 1237 (1990).
[13]B. LaBombard and L. Lyons, Review of Scientific Instruments **78**, 073501-073501-9 (2007).
[14]M. Mitov, A. Bankova, M. Dimitrova, P. Ivanova, K. Tutulkov, N. Djermanova, R. Dejarnac, J. Stöckel, and T. K. Popov, in *Journal of Physics Conference Series*, Journal of Physics Conference Series, Vol. 356 (2012) p. 012008.
[15]W. Bussière, Journal of Physics D Applied Physics **34**, 1007 (2001).
[16]J. Boedo, G. Gunner, D. Gray, and R. Conn, Review of Scientific Instruments **72**, 1379 (2001).
[17]J. Horacek, R. A. Pitts, and J. P. Graves, Czechoslovak Journal of Physics **55**, 271 (2005).
[18]C. Theiler, B. Lipschultz, J. Harrison, B. Labit, H. Reimerdes, C. Tsui, W. A. J. Vijvers, J. A. Boedo, B. P. Duval, S. Elmore, P. Innocente, U. Kruezi, T. Lunt, R. Maurizio, F. Nespoli, U. Sheikh, A. J. Thornton, S. H. M. van Limpt, K. Verhaegh, N. Vianello, the TCV Team, and the EUROfusion MST1 Team, Nuclear Fusion **57**, 072008 (2017).
[19]H. Reimerdes, B. P. Duval, J. R. Harrison, B. Labit, B. Lipschultz, T. Lunt, C. Theiler, C. K. Tsui, K. Verhaegh, W. A. J. Vijvers, J. A. Boedo, G. Calabro, F. Crisanti, P. Innocente, R. Maurizio, V. Pericoli, U. Sheikh, M. Spolare, N. Vianello, the TCV Team, and the EUROfusion MST1 Team, Nuclear Fusion **57**, 126007 (2017).
[20]A. Fasoli and al., Proc. 27th IAEA Fusion Energy Conference, Gandhinagar, India, October 22-27 , paper FIP/P8 (2018).